Desalination and Water Treatment
www.deswater.com

doi: 10.5004/dwt.2020.24879

174 (2020) 230–239
January

Effective removal of trace antimony(III) from aqueous solution by phosphonic acid-functionalized hollow mesoporous silica spheres as a novel adsorbent

Yao Yan[a], Jing-song Wang[a,*], Si-li Chen[b], Yong-xin Bing[b,*], Qing-wei Guo[b], Zhi-yong Duan[a], Lei Xie[a], Ke-chang Han[a]

[a]*School of Civil Engineering, University of South China, Hengyang 421000, China, Tel. +(0734)8282449; Mob. +13017168579; email: xhwjs@163.com (J.-s. Wang), Mob. +18692208098; emails: yaoyoung93@163.com (Y. Yan), zd9@msstate.edu (Z.-y. Duan), Mob. +15367340321; email: 708801343@qq.com (L. Xie), Mob. +15886444751; email: 708801343@qq.com (K.-c. Han)*
[b]*South China Institute of Environmental Sciences, Ministry of Environment Protection, Guangzhou 510655, China, Tel: +13512720676; emails: chensili@scies.org (S.-l. Chen), 411152790@qq.com (Y.-x. Bing), Mob. +13512720676; email: qwguo16@163.com (Q.-w. Guo)*

Received 27 May 2018; Accepted 9 September 2019

ABSTRACT

This study focused on the preparation of phosphonic acid-functionalized hollow mesoporous silica spheres (PHMSs) and their adsorption performance of trace antimony(III) from water under room temperature. Firstly, monodisperse carbon microspheres (CS) synthesized by the glucose-oxygen hydrothermal method was used as the hard template, and cetyltrimethylammonium bromide as the soft template to synthesize hollow mesoporous silica spheres (HMSs). Then, phosphate groups were grafted by the post-grafting method to synthesize PHMSs. The characterization of the materials was investigated by scanning electron microscopy, Fourier-transform infrared spectroscopy, transmission electron microscopy methods, and Beckman Laser laser particle size analyzer. The results showed that PHMSs have a regular mesoporous structure, monodisperse particle size distribution, and a stable shell-core structure. The CS synthesized in this study with glucose precursors is superior in the uniformity of particle size to sucrose and starch precursors. The addition of ammonia could accelerate the hydrothermal polymerization of carbon microspheres during the hydrothermal reaction. The reducing conditions provided by the hydrothermal heat promoted the carbonization reaction and increased the average particle size of the carbon microspheres from 395 nm to 11.5 μm. The average pore size of the synthesized HMSs is 2.5 nm. The hollowness of the hollow spheres can be controlled by adjusting the particle size of the hard template. The content of each component in the reaction system has a great influence on the shell thickness and pore size of the formed HMSs. Infrared spectroscopy showed that on the surface of HMSs, the phosphate groups were highly compatible with the silanol groups. The adsorption experiment results showed that PHMSs have high adsorption of Sb(III) with an initial concentration of 100 μg L^{-1} and can be used as an effective adsorbent for trace amounts of antimony(III) in water. The maximum adsorption capacity is 87.46 mg g^{-1}, the maximum removal rate is 96.02% and the adsorption equilibrium time is 6 h. The fitting degree of the Langmuir equation is 99.96%, indicating that the chemical adsorption is the main adsorption mechanism.

Keywords: Trace antimony(III) adsorption; Hollow mesoporous silica spheres; Phosphonic acid-functionalized silica; Hard and soft templet method

1. Introduction

Antimony (Sb) is widely used in various products, such as batteries, flame retardants, textiles, plastics, ammunition and glass decolorizers [1]. Antimony and its compounds have been regarded as priority pollutants by the United States Environmental Protection Agency (USEPA) and the European Union (EU) [2]. To reduce the potential health

* Corresponding author.

risks of Sb(III), an increasingly strict drinking water standard for Sb has been promulgated in many countries [3,4]. Drinking water maximum contaminant level of Sb is regulated as 6 μg L^{-1} by USEPA, and set as 5 μg L^{-1} in the EU and China. Although the concentration of Sb in natural waters is normally less than 1 μg L^{-1} [5], large quantities of antimony have been released into the environment in contaminated locations, especially shooting ranges, mining and smelting industrial sites [6]. Therefore, it's imperative to develop efficient technologies to remove trace Sb(III) from water.

Several methods, including reverse osmosis [7–9], coagulation/flocculation [10], electrolytic reduction [11], biological reduction and precipitation [12] and adsorption [13] have been used for the removal of Sb ions from aqueous solutions. Among these methods, the adsorption method is one of the most preferred techniques for the remediation of heavy metal ions from aquatic systems, owing to its advantage of cost-effectiveness, simplicity and rapidness of operation, small sludge yield, high efficiency and renewability [14–16].

Various types of natural, modified and synthesized materials[17,18] such as activated carbon [19], multi-walled carbon nanotubes [20], oxide of iron and aluminum [21], magnetic nanoparticles [22] and *Microcystis* [23] have been employed as adsorbents to remove Sb(III) from water. Compared with those materials, hollow mesoporous silica spheres (HMSs) can serve as a more ideal shell component, owing to its stability under acidic conditions, the inertia to redox reactions, and the abundance of surface hydroxyl groups, those characteristics make it easy for surface modification [24]. Moreover, the particular structure and practical behaviors, such as nontoxicity, large steerable inner pore volume, high mechanical strength, and penetrable porous matrix wall could also increase grafting site, thus augmenting the modification efficiency.

The grafting of new functional groups on silica-based sorbents may increase the density of adsorption sites, change the mechanism of adsorption, broaden the range of pH for efficient adsorption and increase the selectivity for target metals. There are mainly two kinds of grafting methods for mesoporous materials, after-grafting method and copolymerization method. The post grafting method has a weak influence on the structure of the mesoporous, the content of organic functions distributed on the outer surface by post grafting method is generally higher than the copolymerization method [25]. The phosphonic acid groups were often found to be superior to other inorganic substrates, because of the higher robustness and stability of metal-OP over metal-OSi bonds [26]. Also, the phosphonic acid group showed high compatibility with other organic functional groups, a feature that made it efficient for surface modification, so they could be performed in many solvents including water [27].

Herein, in this article, we report phosphonic acid-functionalized hollow mesoporous SiO_2 microspheres (PHMSs) as a novel adsorbent for the adsorption of trace antimony(III) from aqueous solution. Firstly, we prepared HMSs with hard (carbon spheres) and soft (cetyltrimethylammonium bromide (CTAB)) templet method, to provide an ideal shell phosphonic acid group carrier. Secondly, we synthesized PHMSs by binding phosphonic acid group onto HMSs using the after-grafting method, the obtained spheres maintained the structure of mesoporous well and showed an increasing number of the binding site for antimony(III) adsorption compared with HMSs. Finally, The application of the resulting functional materials for the removal of trace antimony(III) from aqueous solution was conducted, the uptake kinetics and adsorption isotherms for Sb(III) adsorption onto PHMSs were evaluated.

The innovations of this research are as follows: HMSs were prepared with excellent structure and properties and realized the regulation of their particle size. It was the first attempt that modified HMSs with phosphate groups used as antimony adsorbents, and its adsorption performance for the treatment of trace antimony(III) from the water was being explored. HMSs modified with phosphate groups, which gave more physical and chemical characteristics to them, and the hollow structure made the silicon spherical materials more modifiable.

2. Experimental section

2.1. Chemicals and reagents

Glucose, ammonia solution (25%–28%), ethanol, tetraethyl orthosilicate (TEOS), acetic acid, NaOH and toluene were purchased from Sigma-Aldrich (America). CTAB was purchased from Tokyo Chemical Industry Co. Ltd., Japan. Antimony trioxide, diethylphosphatoethyltriethoxysilane, $(C_2H_5O)_3Si(CH_2)_2P(O)(OC_2H_5)_2$ (DPTS) were purchased from Gelest Inc., USA. All materials were used without further purification, and deionized water was used in all research.

2.2. Sample preparation

2.2.1. Preparation of CSs

CSs were made from glucose with the hydrothermal method. In a typical synthesis procedure, 6, 7, 8, 9, and 10 g of glucose was dissolved in 70 mL deionized water until clear solutions. Next, the clear solution was added different amount of ammonia, 0.01, 0.02, 0.03, 0.04, 0.05, and 0.06 mol L^{-1}, treated with flowing N_2 of 200 mL min^{-1} for 30 min. And then, the solution was transferred into a stainless-steel autoclave (100 mL) to be heat-treated at 220°C for 8, 9, 10, 11, and 12 h for the hydrothermal reaction. After being cooled down to room temperature and centrifugation process, the as-received black rinsed with water and ethanol for three cycles. Vacuum drying oven was used under 80°C for 12 h, the precipitate was then identified as CSs.

2.2.2. Preparation of HMSs

The optimal CSs (0.7 g mL^{-1} glucose solution heat-treated for 12 h) were taken as a precursor. The resultant CSs (0.3 g) was soaked in 10 mL NaOH solution (1 M) at 80°C with rotating speed 150 rpm in a constant temperature oscillator to get the surface modification. After this step, the CSs were added in the mixture of ethanol (71.4 mL), H_2O (10 mL) and ammonia solution (1.57 mL), CTAB (0.01, 0.05, 0.1, 0.2, and 0.3 g), the dropwise addition of TEOS (0.035, 0.07, 0.14, 0.28, and 0.56 g) were after the mixture solution being homogenized in ultrasound cell breaker for 10 min, the adding process with continuous ultrasonic dispersion for 20 min. Rinsing

and drying procedure was the same as the CSs, hard and soft template removing were calcined at 700°C for 6 h.

2.2.3. Preparation of PHMSs

2.5 mmol (0.8 mL) DPTS was pre-hydrolyzed in 23.5 mL concentrated acetic acid at 80°C for 6 h with reflux condensing and oil bathing. The mixed solution was then cooled down to room temperature. After adding 1.0 g optimal HMSs (0.549 mmol CTAB and 1.34 mmol TEOS) and 50 mL toluene to refluxing, methanol ethanol cycle washing was then conducted. Desiccation was in a vacuum drying oven for 12 h at 70°C.

2.3. Trace antimony(III) sorption experiments

100 μg L^{-1} of trace antimony(III) sorption experiments were conducted for 1 to 4 h by different concentrations (1, 1.2, 1.4, 1.6, 1.8, and 2.0 mg L^{-1}) of PHMSs adsorbent at initial pH of 1.0 to 7.0 under room temperature. The quantification of the remaining antimony(III) in solution was determined by the atomic fluorescence spectrometer.

2.4. Characterization of the sorbents

The morphology of the spheres was observed by a Zeiss Supra 40 (Germany) scanning electron microscopy (SEM) at the accelerating voltage of 10.0 kV. Transmission electron microscopy (TEM) images were obtained on a Tecnai FEI G2 F30 electron microscope operating at 200 kV (Netherlands). Fourier-transform infrared spectroscopy (FTIR) spectra were measured on a Nicolet, Magna-550 spectrometer using KBr tablet. Analysis of particle size distribution was tested by the Beckman Laser particle size analyzer and was also calculated from desorption branches of isotherms by the Barrett–Joyner–Halenda (BJH) method. Pore volume and specific surface area were calculated using BJH and Langmuir methods, respectively [28].

3. Results and discussion

3.1. Characterization of materials

The synthesis procedure is shown in Fig. 1. Firstly, the prepared monodisperse CSs by the hydrothermal method were treated by alkali solution to increase the hydrophilicity of the surface. Secondly, the CS@m SiO_2/CTAB composites were obtained with CTAB as a soft template. Thirdly, the CTAB and CSs were removed by calcination to form the mesoporous silica shell and hollow core. Also, the hydrothermal treatment was in favor of formatting a hydroxy-coated surface. Finally, the DPTS addition resulted in well-dispersed hollow mesoporous phosphonic acid-functionalized silica spheres.

Monodisperse carbonaceous spheres were prepared by the hydrothermal process, the decomposition of glucose is intricacy especially with NH_4^+ addition [29,30]. It is known that formaldehyde reacts with the ammonia in no time, generating an active amino group [31], described in Fig. 2. NH_4^+ has a significant influence on the morphology and size of the synthesized spheres. In the reaction of NH_4^+ and the C=O group, more active hydroxyl and branches in the molecular chains promote polymerization, schematic diagram as Fig. 3

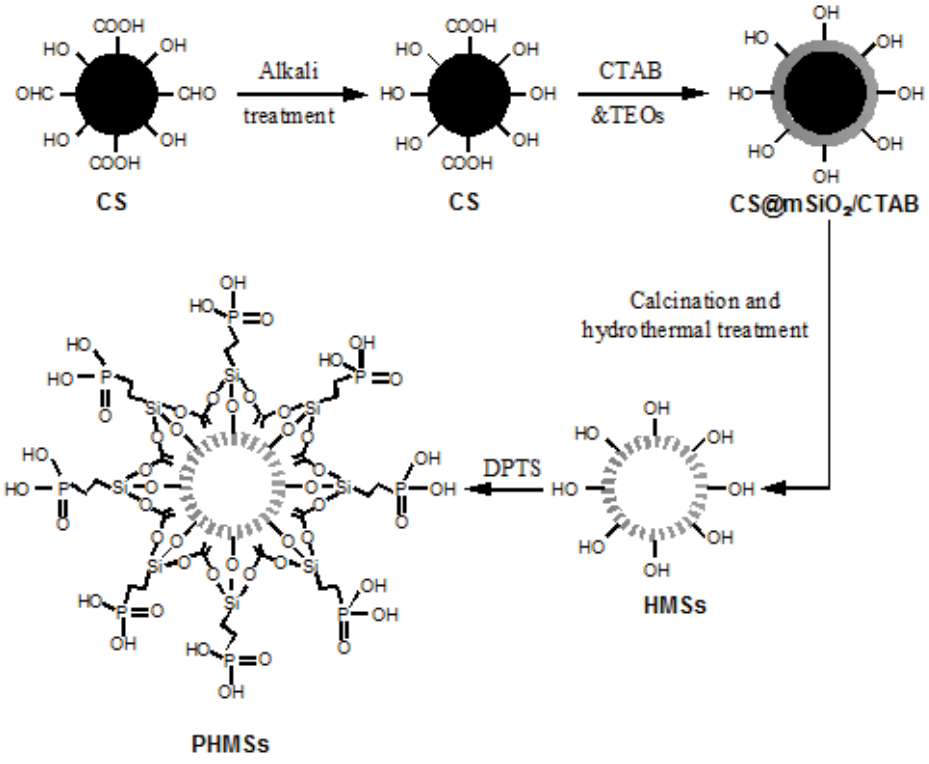

Fig. 1. Synthesis of PHMSs (the scales are arbitrary and do not respect the real dimensions).

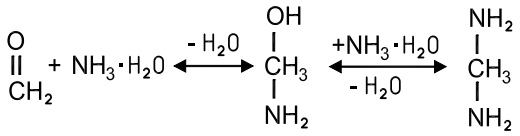

Fig. 2. Auxiliary reaction principal of $NH_3 \cdot H_2O$.

[32], which could make the spheres grow bigger and increase the silicon dioxide binding site.

The result showed that 0.7 g mL^{-1} glucose solution heat-treated for 12 h could formate the best morphology of CSs as shown in Fig. 4. The products (Fig. 4a) synthesized without ammonium addition have a smaller size, while the particles were easy to agglomerate. When the NH_4^+ concentration increases to 0.06 mol L^{-1}, the CSs have a tremendous change from 0.2 to 13.6 μm in average diameter while the surface was loose and smooth (Fig. 4b). As we know, the anaerobic

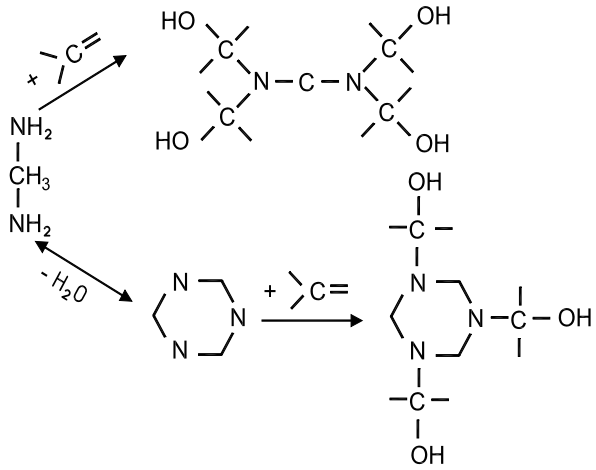

Fig. 3. Active hydroxyl and branches in the molecular chains.

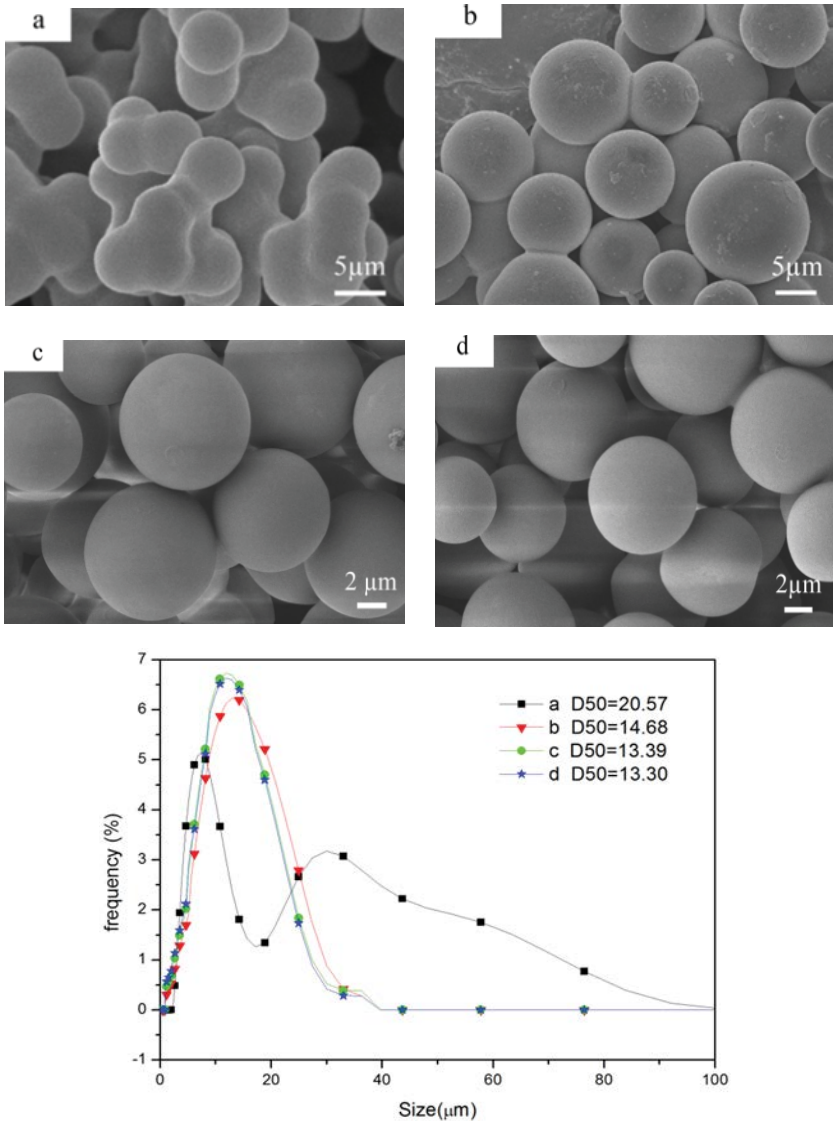

Fig. 4. SEM photographs and particle size distributions of CSs which were (a) no ammonium addition, (b) 0.06 mol L^{-1} ammonium addition, (c) 0.06 mol L^{-1} ammonium addition and oxygen-free environment, and (d) soaked in NaOH solution.

environment is beneficial to a reduction reaction, and CSs treated with flowing N_2 resulted in its particle size distribution more concentrated (Fig. 4c). The CSs soaked in NaOH solution become more negatively charged with cracks, and the C=O groups decrease owning to the alkali solution react with the C=O groups which will correspondingly increase the hydrophilicity of the surface of CSs (Fig. 4d), therefore, it's easier to combine with silicon hydroxyl.

With the increase of the alkali treatment time of the CSs, the zeta potential becomes more negative [33]. The surface of the CSs contain several characteristic absorption bands at 3,450 cm^{-1} (O–H stretching), 2,931 cm^{-1} (–CH_2), 1,637 cm^{-1} (C=O stretching), 1,381 cm^{-1} (C=O stretching), 1,023 cm^{-1} (characteristic furan), and 803 cm^{-1}(aromatic ring) in all the samples, which conformed with the previous reports [34,35]. The two peaks at 1,637 and 1,381 cm^{-1} were not obvious the sample *b* but occurred in the sample without ammonium addition. Since the absorptions at 1,637 and 1,381 cm^{-1} correspond to C=O, in the –COOH stretching mode, the disappearance of the two peaks in sample *b* implies some reaction of C=O under the action of NH_4^+. However, during calcination, the HMSs aggregated and a considerable Si–OH (Silanol group) is lost. To reduce this loss, hydrothermal treatment was employed after calcination (Fig. 5).

After the coating of the SiO_2 layer at the surface and successive removal of the template, mesoporous hollow silica shells were prepared (Fig. 6). TEM images of microtomed particles confirm the hollow interior of the particles and the mesoporous shell, and the morphology of the particle size distribution was largely improved. All of those proved that the particles were favorable for phosphonic acid loading (Fig. 6a). The surface modification of PHMSs with DPTS could be identified from the TEM image faintly since the grafted-DPTS layer on the surface of the hollow spheres was quite thin. Yet, TEM images of PHMSs show that the particles were completely hollow in the inner core, and the surface was much rougher than before, indicating it's suitable for absorption enhancement (Fig. 6b).

As the infrared spectra are shown in Fig. 7a, two apparent absorption bands observed at 3,444 and 1,640 cm^{-1} were associated with –OH stretching and bending vibrations on the surface silanol groups with a hydrogen bond. From Figs. 7a and b can be observed that –OH stretching was shifted to higher frequencies, indicating hydroxy recovery resulted from hydrothermal treatment. For all samples, typical absorption peaks around 800 and 1,080 cm^{-1} were observed, which were associated with the stretching vibrations of Si–O–Si and Si–O, respectively [36]. After the modification of phosphonic acid, some new characteristic peaks appeared in the spectra for PHMSs (Fig. 7c). The peak at 1,220 cm^{-1} was attributed to the P=O stretching vibration of the *P*-containing groups. The peak at 1,640 cm^{-1} was due to water bending [37]. The band of medium intensity, which corresponds to vibrations (Si–CH_2) was identified in this region at 1,405–1,456 cm^{-1} [38]. Thus, it can be concluded that the surface layer of PHMSs contains phosphonic acid groups –$(CH_2)_2P(O)(OH)_2$, which were raised from the hydrolyzation of DPTS. Thus the phosphonic acid functional groups had been anchored onto the surface of silica successfully. After trace antimony(III) adsorption, almost all kinds of functional groups bring into correspondence with before (Fig. 7d), declared the stability and reusability of this material. A nitrogen sorption isotherm measured for CSs is shown in Fig. 8a, the particles had a Brunauer–Emmett–Teller surface area of 984 $m^2\ g^{-1}$. Pore size distribution

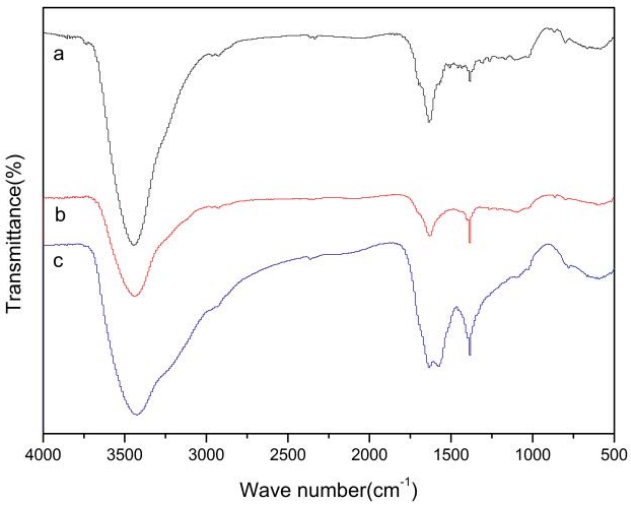

Fig. 5. FTIR spectra of (a) CSs without ammonium addition, (b) with 0.06 mol L^{-1} ammonium addition and oxygen-free environment, and (c) CSs treated by NaOH solution for 8 h.

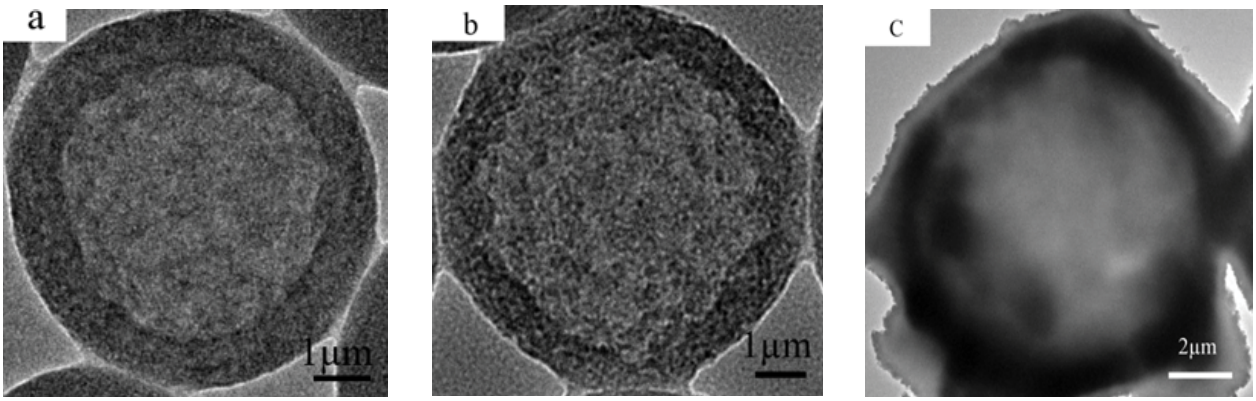

Fig. 6. TEM image of (a) HMSs, PHMSs before, (b) and after, (c) trace antimony(III) adsorption.

analysis showed the macroporous of the spheres, which was peaking at about 29 nm. The isotherm is shown in Fig. 8b has the characteristic features of Type IV isotherms [39], with well-developed H1 type hysteresis loops which were related to the capillary condensation in mesopores, this figure showing the mesoporous structure of all HMSs samples. Correspondingly, the pore diameter distribution of the samples showed a narrow pore distribution with a peak value of 2.5 nm. Though the small and large pores correspond to the mesopores across the shell and in the interior hollow cavities of the individual capsules respectively, the BJH method couldn't analysis the pores with several microns [40]. N_2 adsorption–desorption isotherms show a distinct decrease of hysteresis loops after the phosphonic acid encapsulation, indicating the successful loading of phosphonic acid. While the well-defined mesostructures of HMSs were still maintained, pore size distribution decreased slightly, which was peaking at 2.3 nm(Fig. 8c).

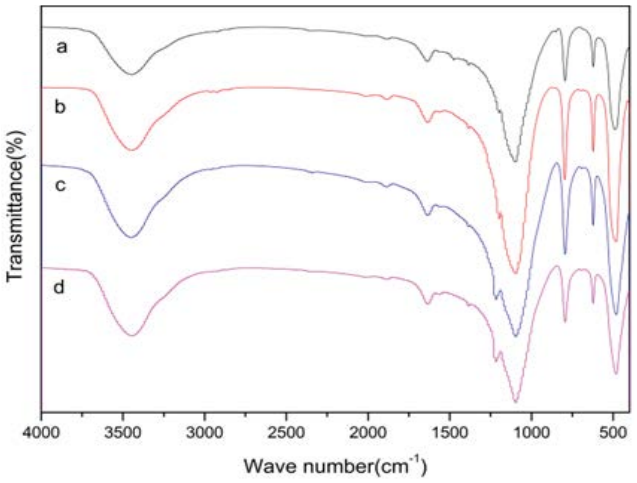

Fig. 7. FTIR spectra of HMSs before (a) and after (b) hydrothermal process; PHMSs before(c) and after (d) trace antimony(III) adsorption.

3.2. Factors affecting adsorption

The removal rate curves for antimony(III) using PHMSs are shown in Figs. 9–11. It can be seen that the removal rate (%) increases from 87.46 to 96.02 (adsorption capacity 87.46 mg g^{-1}) as the initial PHMSs concentration (C_p) increases from 1 to 2 mg L^{-1}. Increasing PHMSs concentration increased the possibility of interaction of antimony(III) species with the high energy active sites, thus enhancing trace antimony(III) uploading (Fig. 9). The amount of antimony(III) adsorption increases rapidly in the first 60 min of contact time and thereafter it proceeds at a slow rate and finally maintains the level. The initial stage corresponds to the

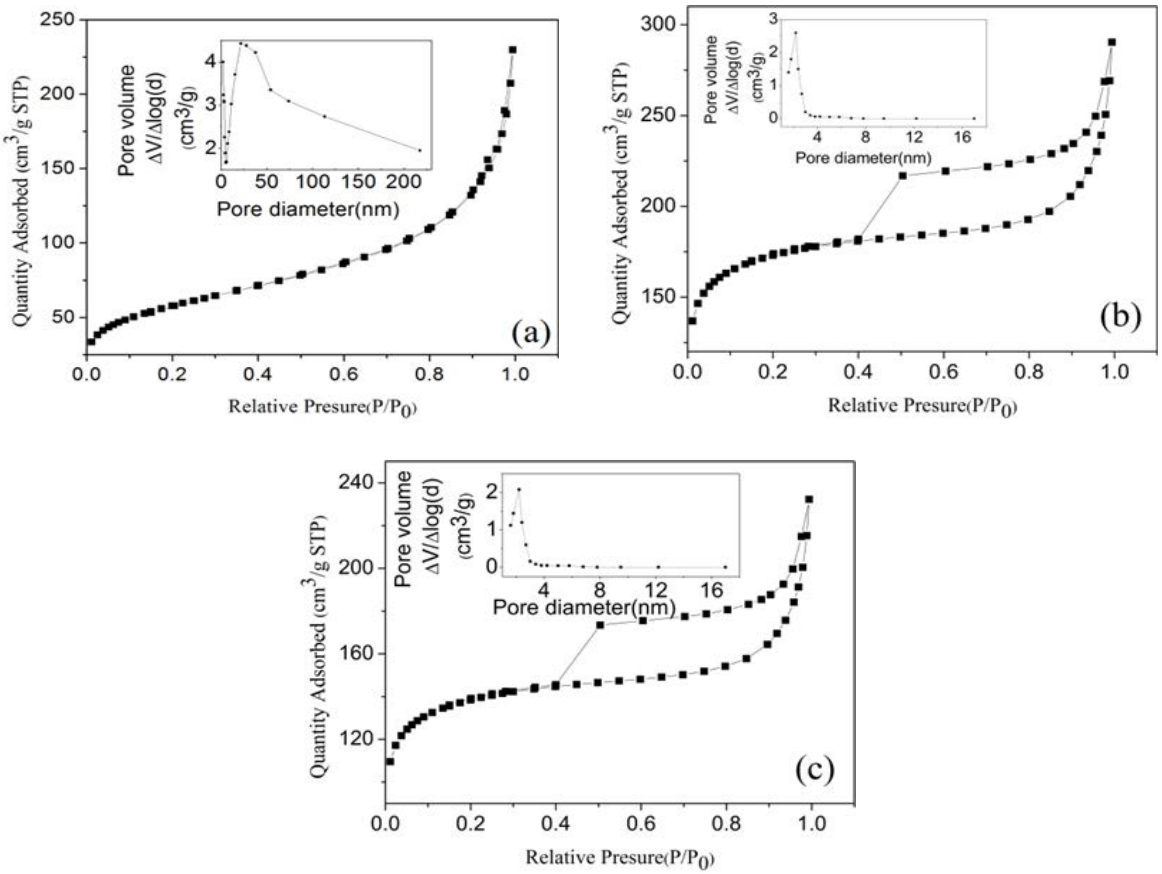

Fig. 8. Nitrogen adsorption-desorption isotherms and BJH pore size distribution of samples (a) CSs, (b) HMSs, and (c) PHMSs.

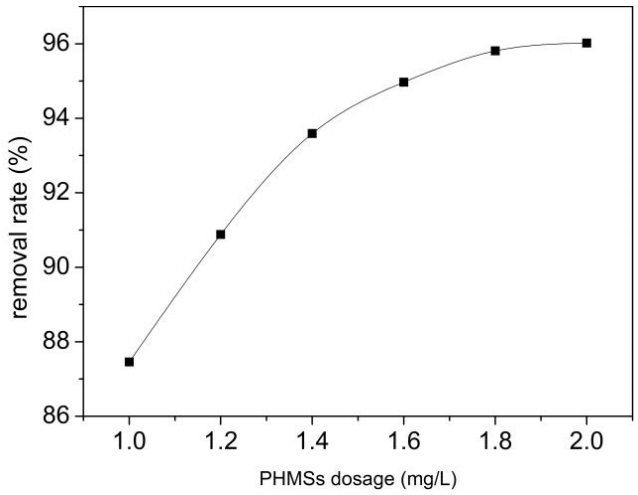

Fig. 9. Effect of antimony(III) removed by different adding amount of PHMSs (pH 6.0, T = 298 K, t = 60 min, C_p = 1–2 mg L^{-1}).

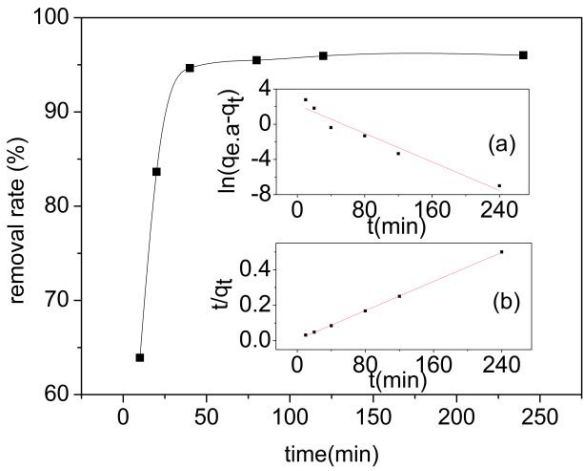

Fig. 10. Effect of contact time on the removal rate of Sb(III) ions by PHMSs (pH 6.0, T = 298 K, t = 1–4 h, C_p = 2 mg L^{-1}).

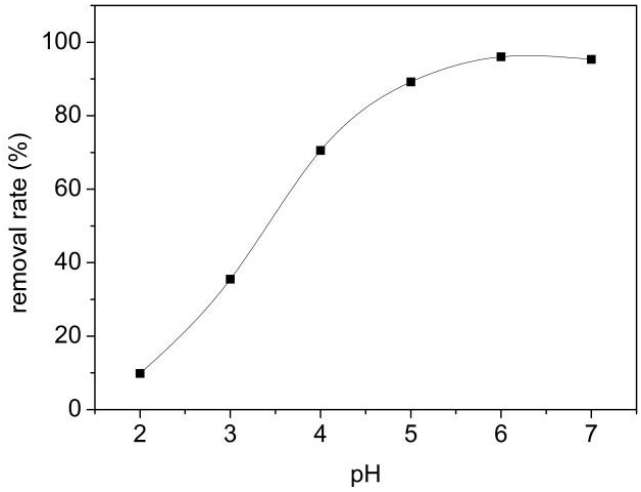

Fig. 11. Effect of pH on antimony(III) adsorption onto PHMSs (pH 1.0–7.0, T = 298 K, t = 60 min, C_p = 2 mg L^{-1}).

fast adsorption of antimony(III) due to the strong affinity of reactive phosphonic acid groups on PHMSs for antimony(III) adsorption. The second step in the process corresponds to slow adsorption limited by the decrease in the availability of both antimony ions in solution and un-occupied adsorption sites of the sorbents. Based on these results a contact time of about 60 min was sufficient to achieve steady-state (Fig. 10). The removal rates of trace antimony(III) were also explored, under the experimental conditions of acid-to-neutral pH values, T = 298 K, t = 60 min and C_p = 2 mg L^{-1}, as shown in Fig. 11. The removal rate increased with the increase of pH value at pH 2–6. While the removal rate decreased slightly at pH 7, indicated the weakly acidic condition of pH 6 conducive to the removal of antimony(III) by PHMS.

3.3. Adsorption curve

Fig. 12 shows the adsorption isotherm for antimony(III) onto PHMSs at initial pH = 6.0, T = 298 K, t = 6 h, C_p = 2 mg L^{-1}. As the equilibrium concentration of antimony(III) increases, the adsorption capacity (q_e) increases. Adsorption equilibrium data were analyzed using the Langmuir model and the Freundlich model, respectively. The Langmuir model was used to describe homogeneous monolayer adsorption and is expressed as Eq. (1):

$$\frac{C_e}{q_e} = \frac{C_e}{q_m} + \frac{1}{q_m K_L} \tag{1}$$

In this equation, q_m is the adsorption capacity of the sorbent when the monolayer is saturated (mg g^{-1}); K_L is the Langmuir adsorption constant (L mg^{-1}). The Freundlich model is usually applied to heterogeneous adsorption, as in Eq. (2):

$$\ln q_e = \ln K_F + \frac{1}{n} \ln C_e \tag{2}$$

In this equation, K_F is the Freundlich isotherm constant, and n (dimensionless) is the heterogeneity factor.

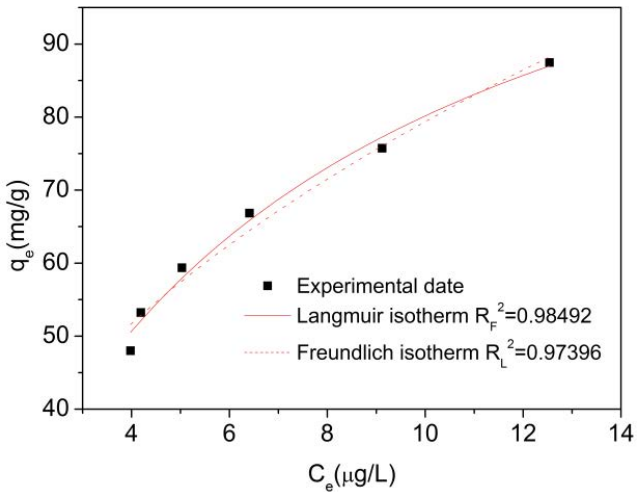

Fig. 12. Adsorption isotherms of antimony(III) on PHMSs.

The parameters of the models are summarized in Table 1. The solid lines in Fig. 11 shows the modeling results of Langmuir adsorption isotherms. The simulated curves are close to experimental points as a confirmation of the suitability of the Langmuir equation to fit adsorption isotherms. The value of the exponential term (i.e., 1/*n*) for Freundlich model was less than the unity, and thus the system can be considered as favorable for trace antimony(III) adsorption [41]; however, the correlation coefficient was lower than in the case of the Langmuir equation. The results suggesting that trace antimony(III) absorbed to form a monolayer coverage and chemisorption was the predominant adsorption mechanism, which was consistent with the strong chelation between antimony(III) ions and phosphonic acid groups on PHMSs.

The kinetic data were modeled using various models such as the pseudo-first-order model, the pseudo-second-order model [42] and the intra-particle diffusion model. They could be expressed by Eqs. (3)–(5), respectively:

$$\ln\left(q_e - q_t\right) = \ln q_e - k_1 t \tag{3}$$

$$\frac{t}{q_t} = \frac{1}{k_2 q_e^2} + \frac{1}{q_e} t \tag{4}$$

$$Q_t = K_{\mathrm{id}} t^{0.5} + X \tag{5}$$

In these equations, k_1 is the pseudo-first-order model rate constant (min^{-1}); k_2 is the pseudo-second-order rate constant (g mg^{-1} min^{-1}); K_{id} is the intraparticle diffusion rate constant (mg g^{-1} min^{-1}); q_e and q_t (mg g^{-1}) are the Sb(III) adsorbed amounts at equilibrium; X is boundary layer (liquid film) thickness (mg g^{-1}) and time t (h), respectively. Table 2 shows the parameters of the model and its correlation coefficients. It can be seen that the best fitting of experimental data corresponds to the pseudo-second-order: the kinetics of Sb(III) adsorption on PHMSs obeys the pseudo-second-order kinetic equation. The fitting diagram based on pseudo-second-order is also shown in Fig. 10. (the insert figure). These results indicate that the dominant mechanism for Sb(III) adsorption on PHMSs was: Chemical adsorption or strong chelation of the phosphonic group. The pseudo-first-order model shows a poor correlation coefficient, indicating that the relevant mechanism does not play an important role in controlling adsorption kinetics. Fig. 13 and Table 2 show that the linear regression curve is not a straight line and do not pass through the origin, the particle inter-diffusion model fits the adsorption poor, the correlation of linear regression equations (R^2) is small. They indicate that the adsorption process speed is not only controlled by inter-diffusion speed but jointly by chemical adsorption and intraparticle diffusion.

Table 1
Parameters of the Langmuir and Freundlich models for antimony(III) adsorption on PHMSs

Sorbent	Langmuir		
	q_m (mg g^{-1})	K_L (L mg^{-1})	R^2
PHMSs	117.638	0.15139	0.98063
Sorbent		Freundlich	
	K_F (mg^{1-n} L^n g^{-1})	n	R^2
PHMSs	110.726	–0.20764	0.97908

Table 2
Kinetic parameters of antimony(III) adsorption onto PHMSs

C_0 (μg L^{-1})	Pseudo-first-order model		
	K_1	$q_{e,a}$	R^2
100	–0.4051	2.19866	0.97693
C_0 (μg L^{-1})	Pseudo-second-order model		
	K_2	$q_{e,a}$	R^2
100	0.0205	0.00598	0.99961
C_0 (μg L^{-1})	Intra-particle diffusion model		
	K_{id}	X	R^2
100	1.02166	35.70278	0.37926

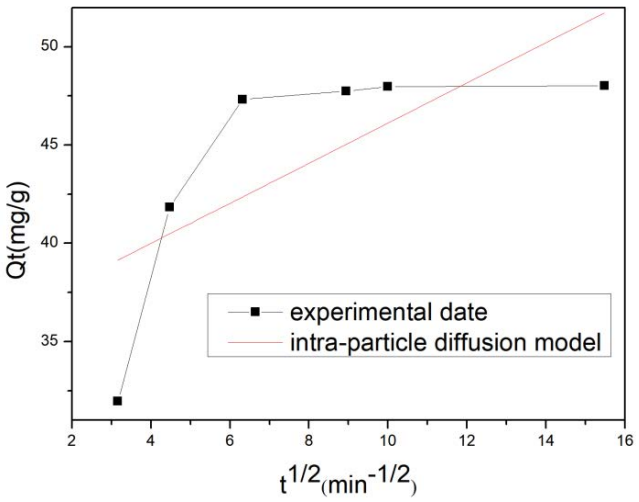

Fig. 13. Intra-particle diffusion model curve of antimony(III) on PHMS.

4. Conclusions

In this study, a novel adsorbent PHMSs has been synthesized, characterized and efficiently tested for trace antimony(III) adsorption from aqueous solution.

- The hard and soft templet method proved to be an effective method for the synthesis of HMSs with an average pore size of 2.5 nm. The hollow spheres possess radially aligned mesochannels and the internal hollow core size could be regulated by adjusting the particle size of the hard templet.
- The phosphonic acid group showed high compatibility with silicon hydroxyl on the surface of HMSs, supported by the FTIR spectra. The N_2 adsorption–desorption isotherms indicated that the pore size distribution of HMSs with well-defined mesostructures is peaking at ~2.3 nm, suggesting the phosphonic acid group was loaded successfully.

- The maximum adsorption capacity was found to be 87.46 mg g^{-1} for trace antimony(III) adsorption at pH 6.0, PHMSs concentration 2.0 mg L^{-1} and initial antimony(III) concentration 100 μg L^{-1}, at room temperature. The Langmuir equation fitted better with adsorption isotherm compared with the Freundlich model, which declared that chemisorption was the predominant adsorption mechanism. The PHMSs fabricated in this study can serve as a promising, highly efficient and cost-effective adsorbent for removal of Sb(III) from water, and it is especially suitable for drinking water treatment in the case of Sb(III) contamination at trace level.

Acknowledgments

This study was supported by the National Natural Science Foundation (No.21177053,), Hunan Natural Science Foundation (No.2018JJ2324), and Science and Technology Planning Project of Guangdong Province, China (No.2016B020240007).

References

[1] J.A. Ober, U.S. Strontium, Geological Survey Mineral Commodity Summaries, United States Geological Survey, 2013, pp. 156–157.
[2] M.A. Callahan, Water-Related Environmental Fate of 129 Priority Pollutants, Vol. 1, Office of Water Planning and Standards, Office of Water and Waste Management, United States Environmental Protection Agency, 1979.
[3] A.-K. Leuz, C.A. Johnson, Oxidation of Sb(III) to Sb(V) by O_2 and H_2O_2 in aqueous solutions, Geochim. Cosmochim. Acta, 69 (2005) 1165–1172.
[4] T.A. Saleh, A. Sarı, M. Tuzen, Effective adsorption of antimony(III) from aqueous solutions by polyamide-graphene composite as a novel adsorbent, Chem. Eng. J., 307 (2017) 230–238.
[5] M. Filella, N. Belzile, Y.-W. Chen, Antimony in the environment: a review focused on natural waters: II. Relevant solution chemistry, Earth Sci. Rev., 59 (2002) 265–285.
[6] M.C. He, X.Q. Wang, F.C. Wu, Z.Y. Fu, Antimony pollution in China, Sci. Total Environ., 421 (2012) 41–50.
[7] M. Kang, M. Kawasaki, S. Tamada, T. Kamei, Y. Magara, Effect of pH on the removal of arsenic and antimony using reverse osmosis membranes, Desalination, 131 (2000) 293–298.
[8] T.A. Saleh, S.O. Adio, M. Asif, H. Dafalla, Statistical analysis of phenols adsorption on diethylenetriamine-modified activated carbon, J. Cleaner Prod., 182 (2018) 960–968.
[9] T.A. Saleh, V.K. Gupta, Nanomaterial and Polymer Membranes: Synthesis, Characterization, and Applications, ISBN-13 (2016) 978-0128047033.
[10] P. Mondal, S. Bhowmick, D. Chatterjee, A. Figoli, B. Van der Bruggen, Remediation of inorganic arsenic in groundwater for safe water supply: a critical assessment of technological solutions, Chemosphere, 92 (2012) 157–170.
[11] A. Koparal, R. Özgür, Ü.B. Öğütveren, H. Bergmann, Antimony removal from model acid solutions by electrodeposition, Sep. Purif. Technol., 37 (2004) 107–116.
[12] H.W. Wang, F.L. Chen, S.Y. Mu, D.Y. Zhang, X.L. Pan, D.-J. Lee, J.-S. Chang, Removal of antimony (Sb(V)) from Sb mine drainage: biological sulfate reduction and sulfide oxidation–precipitation, Bioresour. Technol., 146 (2013) 799–802.
[13] A. Sarı, G. Şahinoğlu, M. Tüzen, Antimony(III) adsorption from aqueous solution using raw perlite and Mn-modified perlite: equilibrium, thermodynamic, and kinetic studies, Ind. Eng. Chem. Res., 51 (2012) 6877–6886.
[14] T.A. Saleh, A. Sarı, M. Tuzen, Chitosan-modified vermiculite for As(III) adsorption from aqueous solution: equilibrium, thermodynamic and kinetic studies, J. Mol. Liq., 219 (2016) 937–945.
[15] A.A. Alswat, M.B. Ahmad, T.A. Saleh, Zeolite modified with copper oxide and iron oxide for lead and arsenic adsorption from aqueous solutions, J. Water Supply Res. Technol. AQUA, 65 (2016) 465–479.
[16] H.A. Sani, M.B. Ahmad, T.A. Saleh, Synthesis of zinc oxide/talc nanocomposite for enhanced lead adsorption from aqueous solutions, RSC Adv., 110 (2016) 108819–108827.
[17] V.K. Gupta, I. Ali, T.A. Saleh, A. Nayak, S. Agarwal, Chemical treatment technologies for waste-water recycling—an overview, RSC Adv., 16 (2012) 6380–6388.
[18] H.A. Sani, M.B. Ahmad, M.Z. Hussein, N.A. Ibrahim, A. Musa, T.A. Saleh, Nanocomposite of ZnO with montmorillonite for removal of lead and copper ions from aqueous solutions, Process Saf. Environ. Prot., 109 (2017) 97–105.
[19] T.-c. Yu, X.-h. Wang, C. Li, Removal of antimony by $FeCl_3$-modified granular-activated carbon in aqueous solution, J. Environ. Eng., 140 (2014) A4014001.
[20] M.A. Salam, R.M. Mohamed, Removal of antimony(III) by multi-walled carbon nanotubes from model solution and environmental samples, Chem. Eng. Res. Des., 91 (2013) 1352–1360.
[21] X.J. Guo, Z.J. Wu, M.C. He, X.G. Meng, X. Jin, N. Qiu, J. Zhang, Adsorption of antimony onto iron oxyhydroxides: adsorption behavior and surface structure, J. Hazard. Mater., 276 (2014) 339–345.
[22] C. Shan, Z.Y. Ma, M.P. Tong, Efficient removal of trace antimony(III) through adsorption by hematite modified magnetic nanoparticles, J. Hazard. Mater., 268 (2014) 229–236.
[23] F.C. Wu, F.H. Sun, S. Wu, Y.B. Yan, B.S. Xing, Removal of antimony(III) from aqueous solution by freshwater cyanobacteria *Microcystis* biomass, Chem. Eng. J., 183 (2012) 172–179.
[24] M.S. Park, S.M. Seo, I.S. Lee, J.H. Jung, Ultraefficient separation and sensing of mercury and methylmercury ions in drinking water by using aminonaphthalimide-functionalized Fe_3O_4@SiO_2 core/shell magnetic nanoparticles, Chem. Commun., 46 (2010) 4478–4480.
[25] X.H. Wang, G.R. Zhu, F. Guo, Removal of uranium (VI) ion from aqueous solution by SBA-15, Ann. Nucl. Energy, 56 (2013) 151–157.
[26] S. Marcinko, A.Y. Fadeev, Hydrolytic stability of organic monolayers supported on TiO_2 and ZrO_2, Langmuir, 20 (2004) 2270–2273.
[27] C. Queffélec, M. Petit, P. Janvier, D.A. Knight, B. Bujoli, Surface modification using phosphonic acids and esters, Chem. Rev., 112 (2012) 3777–3807.
[28] Y.F. Zhu, W.H. Shen, X.P. Dong, J.L. Shi, Immobilization of hemoglobin on stable mesoporous multilamellar silica vesicles and their activity and stability, J. Mater. Res., 20 (2005) 2682–2690.
[29] C.B. Norris, P.R. Joseph, M.R. Mackiewicz, S.M. Reed, Minimizing formaldehyde use in the synthesis of gold-silver core-shell nanoparticles, Chem. Mater., 22 (2010) 3637–3645.
[30] Q. Liang, J. Chen, Y. Ying, J.-w. Zheng, L.Q. Jiang, Influence of NH_4^+ on the preparation of carbonaceous spheres by a hydrothermal process, J. Mater. Sci., 48 (2013) 3341–3346.
[31] H.H. Richmond, G.S. Myers, G.F. Wright, The reaction between formaldehyde and ammonia, J. Am. Chem. Soc., 70 (1948) 3659–3664.
[32] G.E. Van Gils, Study of the reaction of resorcinol, formaldehyde, and ammonia, J. Appl. Polym. Sci., 13 (1969) 835–849.
[33] R.P. Liu, C.-a, Wang, Synthesis of hollow mesoporous silica spheres with radially aligned mesochannels and tunable textural properties, Ceram. Int., 41 (2015) 1101–1106.
[34] R. Demir-Cakan, N. Baccile, M. Antonietti, M.-M. Titirici, Carboxylate-rich carbonaceous materials via one-step hydrothermal carbonization of glucose in the presence of acrylic acid, Chem. Mater., 21 (2009) 484–490.
[35] J.H. Ryu, Y.-W. Suh, D.J. Suh, D.J. Ahn, Hydrothermal preparation of carbon microspheres from mono-saccharides and phenolic compounds, Carbon, 48 (2010) 1990–1998.
[36] U. Kalapathy, A. Proctor, J. Shultz, A simple method for production of pure silica from rice hull ash, Bioresour. Technol., 73 (2000) 257–262.

[37] K.A. Venkatesan, V. Sukumaran, M.P. Antony, P.R.V. Rao, Extraction of uranium by amine, amide and benzamide grafted covalently on silica gel, J. Radioanal. Nucl. Chem., 260 (2004) 443–450.
[38] M.K. Sureshkumar, D. Das, M.B. Mallia, P.C. Gupta, Adsorption of uranium from aqueous solution using chitosan-tripolyphosphate (CTPP) beads, J. Hazard. Mater., 184 (2010) 65–72.
[39] K.S.W. Sing, D.H. Everett, R.A.W. Haul, L. Moscou, R.A. Pierotti, J. Rouquérol, T. Siemieniewska, Reporting physisorption data for gas/solid systems with special reference to the determination of surface area and porosity, Pure Appl. Chem., 57 (1985) 603–619.
[40] J.H. de Boer, B.C. Lippens, B.G. Linsen, J.C.P. Broekhoff, A. van den Heuvel, Th.J. Osinga, The*t*-curve of multimolecular N_2-adsorption, J. Colloid Interface Sci., 21 (1966) 405–414.
[41] H.-T. Fan, Y. Sun, Q. Tang, W.-L. Li, T. Sun, Selective adsorption of antimony(III) from aqueous solution by ion-imprinted organic–inorganic hybrid sorbent: kinetics, isotherms and thermodynamics, J. Taiwan Inst. Chem. Eng., 45 (2014) 2640–2648.
[42] H. Qiu, L. Lv, B.-c. Pan, Q.-j. Zhang, W.-m. Zhang, Q.-x. Zhang, Critical review in adsorption kinetic models, J. Zhejiang Univ. Sci. A, 10 (2009) 716–724.